TOPOLOGY DESIGN OF COMPLIANT MECHANISMS WITH STRESS CONSTRAINTS BASED ON THE TOPOLOGICAL DERIVATIVE CONCEPT

C.G. LOPES AND A.A. NOVOTNY

Abstract. Compliant mechanisms are mechanical devices composed by one single piece that transforms simple inputs into complex movements. This kind of multi-flexible structure can be manufactured at a very small scale. Therefore, the spectrum of applications of such microtools has become broader in recent years including microsurgery, nanotechnology processing, among others. In this paper, we deal with topology design of compliant mechanisms under von Mises stress constraints. The topology optimization problem is addressed with an efficient approach based on the topological derivative concept and a level-set domain representation method. The resulting topology optimization algorithm is remarkably efficient and of simple computational implementation. Finally, some numerical experiments are presented, showing that the proposed approach naturally avoids the undesirable flexible joints (hinges) by keeping the stress level under control.

1. Introduction

Compliant mechanisms are mechanical devices composed by one single peace that transforms simple inputs into complex movements by amplifying and changing their direction. Hence they are easy to fabricate and miniaturize and have no need for lubrication. Although the concept of compliant mechanisms is not new [11] this kind of multi-flexible structure have received considerable attention in recent years. This fact is due to manufacturing at a very small scale, the introduction of new advanced materials and the fast development of Micro-Electro-Mechanical Systems [14]. Since such microtools are capable to perform precise movements, the spectrum of their applications has become broader including microsurgery, nanotechnology processing, cell manipulation, among others.

In spite of the above mentioned advantages, there are many difficulties in the design process of compliant mechanisms. A compliant mechanism needs to be stiff enough to support external loads and at the same time must be flexible enough to satisfy the kinematic requirements [10]. Another difficulty that arises is the tendency of forming flexible joints (hinges), in which the stresses exceed the material failure limit. In this way, many researchers have addressed the design of hinge-free compliant mechanisms [21, 12, 18, 1, 19, 16], most of them in the context of SIMP and level-set methods. The reader interested in a broader review on topology optimization methods may refer to [14], for instance. However, there are relatively few papers dealing with compliant mechanisms design under stress constraints [1, 19]. According to [15] this is related to the local nature of the stress constraints and to the highly non-linear stress behavior. See for instance the recent paper [13] dealing with stress-constrained topology optimization of compliant mechanisms using the SIMP method, where the stress constraints is enforced by using a normalized global stress measure based on the p-norm of the von Mises effective stress.

In this paper, we deal with topology design of compliant mechanisms under von Mises stress constraints. The topology optimization problem is addressed with an efficient approach based on the topological derivative concept and a level-set domain representation method [6]. In addition, in order to deal with the local stress constraints we follow the original ideas [4], where a class of penalty function is introduced to enforce the point-wise stress constraints. Finally, some numerical experiments are presented, showing that the proposed approach naturally avoids the undesirable hinges by keeping the stress level under control, unlike it occurs in the unconstrained case. The numerical examples agree well with the results that should be expected by other methods. Therefore,

Key words and phrases. Topology Optimization; Topological Derivative; Compliant mechanisms; von Mises stress constraints.

our approach can be seen as an alternative method for optimum design of compliant mechanisms under stress constraints.

In fact, the topological derivative is defined through a limit passage when the small parameter governing the size of the topological perturbation goes to zero. Then, it can be used as a steepest-descent direction in an optimization process like in any method based on the gradient of the cost functional. However, the difficulty in finding a convenient formula of the topological derivative for numerics purposes should be noted. It requires technical derivations strongly dependent on the problem under analysis, which may limit its range of real world applications. On the other hand, in contrast to traditional topology optimization methods, the topological derivative formulation does not require a material model concept based on intermediary densities, so that interpolation schemes are unnecessary. These features are crucial in stress constrained problems, since the difficulties arising from material model procedures are here naturally avoided. In addition, topological derivative has the advantage of providing an analytical form for the topological sensitivity which allows to obtain the optimal design in few iterations. Therefore, the resulting topology optimization algorithm is remarkably efficient and of simple computational implementation, since it features only a minimal number of user-defined algorithmic parameters.

This paper is organized as follows. In Section 2 the problem formulation which we are dealing with is stated. The closed formula for the associated topological derivative is presented in Section 3. In Section 4 some numerical experiments are presented, where a topology optimization algorithm based on the topological derivative and a level set domain representation method is adopted to solve the minimization problem under analysis. Finally, the paper ends with some concluding remarks in Section 5.

2. Problem formulation

We want to find the optimal design of a compliant mechanism subject to von Mises stress constraints into two spatial dimensions. Then, the corresponding optimization problem in which we are dealing with is mathematically stated in what follows.

2.1. The constrained optimization problem.

Let us consider an open and bounded domain $\mathcal{D} \subset \mathbb{R}^2$ and a subdomain $\Omega \subset \mathcal{D}$ with Lipschitz boundary Γ, see sketch in Fig. 2. The boundary Γ is split into two non overlapping subsets, namely, $\Gamma = \Gamma_D \cup \Gamma_N$, where Γ_N consists of three mutually disjoint parts, that is $\Gamma_N = \Gamma_{in} \cup \Gamma_{out} \cup \Gamma_0$. On Γ_D displacements are prescribed, while the input, output and zero boundary tractions are prescribed on Γ_{in}, Γ_{out} and Γ_0, respectively. Given a hold-all domain $\mathcal{D}$ and a stress constraints-enforcement sub-domain $\Omega^\star \subset \mathcal{D}$, the optimization problem consists in finding a subdomain $\Omega \subset \mathcal{D}$ that solves the following constrained minimization problem:

$$\begin{cases} \underset{\Omega \subset \mathcal{D}}{\text{Minimize}}\ \mathcal{F}_\Omega(u) := \beta|\Omega| + \mathcal{J}(u) \\ \text{subject to} \quad \sigma_M(u) \leq \overline{\sigma} \quad \text{a.e. in} \quad \Omega^\star \subset \Omega \end{cases} \tag{2.1}$$

where $\Omega = \Omega^\star \cup \omega \subset \mathcal{D}$, with ω used to denote a part of Ω where the stress constrains are not enforced. Finally, u is solution to the following variational problem: Find $u \in \mathcal{U}$, such that

$$\int_{\mathcal{D}} \sigma(u) \cdot \varepsilon(\eta) = \int_{\Gamma_{in}} q_{in} \cdot \eta + \int_{\Gamma_{out}} q_{out} \cdot \eta \quad \forall \eta \in \mathcal{U}, \tag{2.2}$$

with the space $\mathcal{U}$ defined as

$$\mathcal{U} := \{\varphi \in H^1(\mathcal{D}; \mathbb{R}^2) : \varphi|_{\Gamma_D} = 0\}. \tag{2.3}$$

The idea is to maximize the output displacement u_{out} on Γ_{out} in some direction for a given input traction on Γ_{in}. The exterior medium is represented by springs with stiffness K, attached to the output ports. See details in Fig. 1.

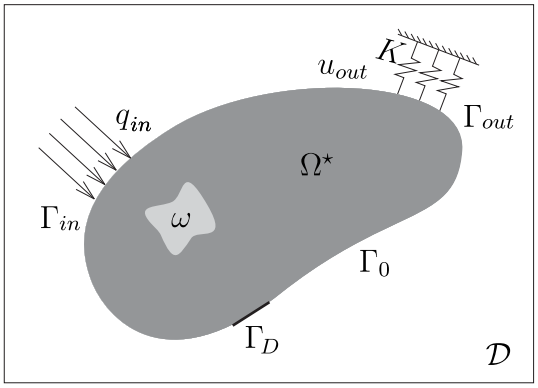

FIGURE 1. Original model.

The springs are then replaced by the expected boundary reaction q_{out} on Γ_{out}. In this way, the output displacement is going to be indirectly constrained by such given reaction. See sketch in Fig. 2.

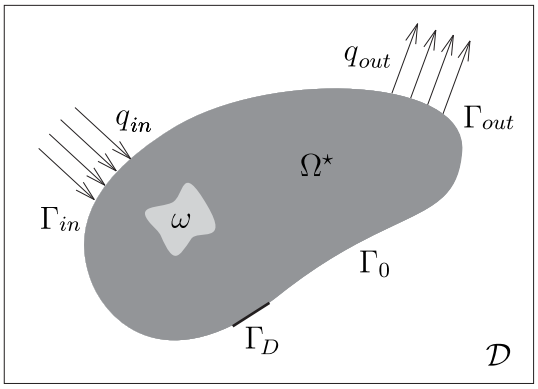

FIGURE 2. Domain representation.

Therefore, the shape functional $\mathcal{J}(u)$ in (2.1) is defined as [6]:

$$\mathcal{J}(u) = \int_{\Gamma_{in}} q_{in} \cdot u + \kappa \int_{\Gamma_{out}} q_{out} \cdot u, \tag{2.4}$$

where q_{in} and q_{out} are given and $\kappa > 0$ is a penalty coefficient.

Some terms in the above expressions still require explanation. The scalar $\beta = \beta^\star/|\mathcal{D}|$, where $\beta^\star > 0$ and $|(\cdot)|$ denotes the Lebesgue measure of $(\cdot)$. The von Mises effective stress $\sigma_M(u)$ is given by

$$\sigma_M(u) := \sqrt{\frac{1}{2}\mathbb{B}\sigma(u) \cdot \sigma(u)} \tag{2.5}$$

with

$$\mathbb{B} = 3\mathbb{I} - \mathrm{I} \otimes \mathrm{I} \tag{2.6}$$

where $\mathbb{I}$ and I are the fourth and second order identity tensors, respectively. The Cauchy stress tensor $\sigma(u)$ and the linearized Green tensor $\varepsilon(u)$ are defined as

$$\sigma(u) = \rho\mathbb{C}\varepsilon(u), \quad \varepsilon(u) = \frac{1}{2}(\nabla u + (\nabla u)^\top), \tag{2.7}$$

with the constitutive tensor $\mathbb{C}$ given by

$$\mathbb{C} = 2\mu\mathbb{I} + \lambda(\mathrm{I} \otimes \mathrm{I}) \tag{2.8}$$

in which μ and λ denote the Lamé's coefficients, both considered constants everywhere. In the plane stress assumption, there are

$$\mu = \frac{E}{2(1+\nu)} \quad \text{and} \quad \lambda = \frac{\nu E}{1-\nu^2}, \tag{2.9}$$

while in plane strain assumption we have

$$\mu = \frac{E}{2(1+\nu)} \quad \text{and} \quad \lambda = \frac{\nu E}{(1+\nu)(1-2\nu)}, \tag{2.10}$$

where E is the Young's modulus and ν the Poisson ratio.

In order to simplify the numerical implementation, we consider that the hold-all domain $\mathcal{D}$ is decomposed into two sub-domains Ω and $\mathcal{D} \setminus \overline{\Omega}$. The domain Ω represents the elastic part while $\mathcal{D} \setminus \overline{\Omega}$ is filled with a very complacent material, used to mimic voids. This procedure allows us to work in a fixed computational domain. Therefore, we introduce a piecewise constant function ρ in (2.7), such that

$$\rho(x) = \begin{cases} 1, & \text{if } x \in \Omega, \\ 0 < \rho_0 \ll 1, & \text{if } x \in \mathcal{D} \setminus \overline{\Omega}, \end{cases} \tag{2.11}$$

with ρ_0 used to mimic voids. That is, the optimization problem, where the structure itself consists of the domain Ω with elastic properties and the remaining empty part $\mathcal{D} \setminus \overline{\Omega}$, is approximated by means of the two-phase material distribution given by (2.11) over Ω. The empty region $\mathcal{D} \setminus \overline{\Omega}$ is filled by a material (the soft phase) with Young's modulus, $\rho_0 E$, much lower than the Young's modulus, E, of the structure material (the hard phase).

2.2. **The penalized optimization problem.** In order to deal with the point-wise stress constraints in (2.1) we use a class of von Mises stress penalty functional introduced in [7].

We start by introducing the nominal stress $S(u)$, defined as

$$S(u) := \frac{\sigma(u)}{\overline{\sigma}}. \tag{2.12}$$

Then, the von Mises stress constraints in terms of normalized stresses is stated as:

$$S_M^2(u) = \frac{1}{2}\mathbb{B}S(u) \cdot S(u) \leq 1. \tag{2.13}$$

We now define the penalized counterpart of objective function in (2.1). Let $\Phi : \mathbb{R}_+ \to \mathbb{R}_+$ be a nondecreasing function of class $\mathcal{C}^2$. We assume that the derivatives Φ' and Φ'' are bounded. The penalty functional is defined as:

$$\mathcal{G}(u) := \int_{\Omega^\star} \Phi(S_M^2(u)). \tag{2.14}$$

In particular, we shall adopt a function Φ of the following functional form (for more details the reader may refer to [7, 8]):

$$\Phi(t) \equiv \Phi_q(t), \tag{2.15}$$

where $q \geq 1$ is a given real parameter and $\Phi_q : \mathbb{R}_+ \to \mathbb{R}_+$ is defined as

$$\Phi_q(t) = [1 + t^q]^{1/q} - 1. \tag{2.16}$$

The exponent q has to be chosen as large as possible. For a detailed explanation on how to choose it we refer to the original paper [4]. Here the exponent q is fixed as $q = 32$.

Therefore, the original constrained optimization problem (2.1) can be approximated by the following penalized unconstrained optimization problem:

$$\underset{\Omega \subset \mathcal{D}}{\text{Minimize}}\ \mathcal{F}_\Omega^\alpha(u) := \mathcal{F}_\Omega(u) + \alpha \mathcal{G}(u), \tag{2.17}$$

with the scalar $\alpha > 0$ used to denote a given penalty coefficient.

3. Topological derivative

The topological derivative was introduced in the fundamental paper [22]. This concept has been successfully applied to solve many relevant problems such as topology optimization, inverse problems, image processing, damage and crack evolution. See, for instance, the book [20].

In this paper, the topological derivative concept is also used to solve the minimization problem (2.17). The topological derivative of the von Mises penalty functional was derived in [7]. The topological asymptotical analysis of the other terms can be found in many references, such as [3, 20].

For the sake of completeness, the topological derivative associated with the objective functional (2.17), with respect to the nucleation of a small circular inclusion of different material property from the background, is here stated in its closed form. Since we are using a very complacent material to mimic voids, the topological derivatives are presented in their limit cases versions when the contrast on the material properties goes to zero or infinity. Note that these limit cases have to be justified. Therefore, the reader may refer to [9], where such cases are discussed together with the concept of degenerated topological derivative. Finally, the results are written in terms of the Lamé's coefficients, so that they can be used either in plane stress or plane strain assumptions.

Theorem 1. *The topological derivative of* (2.17)*, with respect to the nucleation of a small circular inclusion of different material property from the background, is given by the sum*

$$D_T\mathcal{F}^{\alpha}_{\Omega}(u) = \beta D_T|\Omega| + D_T\mathcal{J}(u) + \alpha D_T\mathcal{G}(u). \tag{3.1}$$

We are interested into two cases, which are:
Case 1. *Let us consider $x \in \Omega$. In this case $\rho = 1$ and the contrast on the material property goes to zero since $\rho_0 \ll 1$. Then the topological derivative $D_T\mathcal{G}$ of the von Mises penalty functional reads*

$$\begin{aligned} D_T\mathcal{G}(u) = -\mathbb{P}_0 S(u)\cdot\varepsilon(v) - \chi_{\Omega^\star}k_1(u)\mathbb{T}\mathbb{B}S(u)\cdot S(u) \\ + \frac{1}{4}\chi_{\Omega^\star}k_1(u)(10S(u)\cdot S(u) - 2\mathrm{tr}^2 S(u)) \\ + \chi_{\Omega^\star}\Psi(S(u)) - \chi_{\Omega^\star}\Phi(S^2_M(u)), \end{aligned} \tag{3.2}$$

where the polarization tensor $\mathbb{P}_0$ is written as [2]

$$\mathbb{P}_0 \;=\; \frac{\lambda+2\mu}{\lambda+\mu}\left(2\mathbb{I} - \frac{\mu-\lambda}{2\mu}\mathrm{I}\otimes\mathrm{I}\right). \tag{3.3}$$

The displacements field u is solution to (2.2) *while v is solution to the following variational adjoint problem: Find $v \in \mathcal{U}$, such that*

$$\int_{\mathcal{D}}\sigma(v)\cdot\varepsilon(\eta) = \int_{\mathcal{D}}\chi_{\Omega^\star}k_1(u)\widetilde{\mathbb{B}}S(u)\cdot\varepsilon(\eta) - \int_{\Gamma_{in}} q_{in}\cdot\eta - \kappa\int_{\Gamma_{out}} q_{out}\cdot\eta \quad \forall\eta\in\mathcal{U}, \tag{3.4}$$

with the space $\mathcal{U}$ defined by (2.3) *and the fourth order tensor $\widetilde{\mathbb{B}}$ is given by*

$$\widetilde{\mathbb{B}} = 6\mu\mathbb{I} + (\lambda-2\mu)\mathrm{I}\otimes\mathrm{I}. \tag{3.5}$$

The characteristic function $\chi_{\Omega^\star}$ is written as

$$\chi_{\Omega^\star} = \begin{cases} 1 & \textit{in } \Omega^\star, \\ 0 & \textit{otherwise.} \end{cases} \tag{3.6}$$

The function $k_1(u)$ is defined as

$$k_1(u) = \Phi'(S^2_M(u)) \tag{3.7}$$

and the fourth order tensor $\mathbb{T}$ is written as

$$\mathbb{T} = a_2\mathbb{I} + \frac{a_1-a_2}{2}\mathrm{I}\otimes\mathrm{I} \tag{3.8}$$

with

$$a_1 = \frac{\lambda+\mu}{\mu}; \quad a_2 = \frac{\lambda+3\mu}{\lambda+\mu}. \tag{3.9}$$

At last, the function $\Psi(S(u))$ *can be written as*

$$\Psi(S(u)) = \frac{1}{\pi}\int_0^1\int_0^\pi \frac{1}{t^2}\left[\Phi(S_M^2(u)+\Lambda(t,\theta)) - \Phi(S_M^2(u)) - \Phi'(S_M^2(u))\Lambda(t,\theta)\right] d\theta dt, \tag{3.10}$$

where

$$\Lambda(t,\theta) = -\frac{t}{2}\left[5(S_I^2 - S_{II}^2)\cos\theta + 3(S_I - S_{II})^2(2-3t)\cos 2\theta\right] + \frac{t^2}{4}\left[3(S_I+S_{II})^2 + (S_I-S_{II})^2(3(2-3t)^2 + 4\cos^2\theta) + 6(S_I^2 - S_{II}^2)(2-3t)\cos\theta\right], \tag{3.11}$$

and S_I, S_{II} *are the eigenvalues of* $S(u)$. *Finally, the topological derivative of* $\mathcal{J}(u)$ *is given by*

$$D_T\mathcal{J}(u) = -\mathbb{P}_0\sigma(u)\cdot\varepsilon(v) \tag{3.12}$$

and the topological derivative of the volume reads

$$D_T|\Omega| = -1. \tag{3.13}$$

Case 2. *Now, let us consider* $x \in \mathcal{D}\setminus\overline{\Omega}$. *In this case* $x \notin \Omega^\star$ *by definition and* $\rho = \rho_0 \ll 1$. *Therefore, the contrast on the material property goes to infinity. Then the last term in* (3.1), *namely* $D_T\mathcal{G}$, *is given by*

$$D_T\mathcal{G}(u) = -\mathbb{P}_\infty S(u)\cdot\varepsilon(v), \tag{3.14}$$

with u *and* v *solution to* (2.2) *and* (3.4), *respectively. The polarization tensor* $\mathbb{P}_\infty$ *is written as* [2]

$$\mathbb{P}_\infty = -\frac{\lambda+2\mu}{\lambda+3\mu}\left(2\mathbb{I} + \frac{\mu-\lambda}{2(\lambda+\mu)}\mathrm{I}\otimes\mathrm{I}\right). \tag{3.15}$$

The topological derivative of $\mathcal{J}(u)$ *is given by*

$$D_T\mathcal{J}(u) = -\mathbb{P}_\infty\sigma(u)\cdot\varepsilon(v), \tag{3.16}$$

and, finally, the topological derivative of the volume assumes

$$D_T|\Omega| = 1. \tag{3.17}$$

4. Numerical examples

Some numerical experiments are here presented to show the effectiveness of the proposed methodology. The minimization problem (2.17) is solved by using a topology optimization algorithm based on the topological derivative together with a level-set domain representation method as proposed in [6]. A locally sufficient optimality condition for problem (2.17), under the considered class of domain perturbation given by circular inclusions, can be stated as [5]

$$D_T\mathcal{F}^\alpha_{\Omega^*}(x) > 0 \quad \forall x \in \mathcal{D}\,, \tag{4.1}$$

where Ω^* is a local minimum for problem (2.17). Let us introduce a level-set domain representation function $\psi \in L^2(\Omega)$ of the form:

$$\Omega = \{\psi(x) < 0, \text{ for } x \in \mathcal{D}\}, \tag{4.2}$$

$$\mathcal{D}\setminus\overline{\Omega} = \{\psi(x) > 0, \text{ for } x \in \mathcal{D}\}, \tag{4.3}$$

where ψ vanishes on the interface $\partial\Omega$. We define the quantity

$$g(x) := \begin{cases} -D_T\mathcal{F}^\alpha_\Omega(x), & \text{if } \psi(x) < 0\,, \\ +D_T\mathcal{F}^\alpha_\Omega(x), & \text{if } \psi(x) > 0\,, \end{cases} \tag{4.4}$$

allowing for rewriting the condition (4.1) in the following equivalent form

$$\begin{cases} g(x) < 0, & \text{if } \psi(x) < 0, \\ g(x) > 0, & \text{if } \psi(x) > 0. \end{cases} \tag{4.5}$$

Note that (4.5) is satisfied whenever quantity g coincides with level-set function ψ up to a strictly positive number. Thus, the basic idea consists in finding a fixed point satisfying the following condition

$$\tau > 0 : g = \tau\psi. \tag{4.6}$$

The reader interested in the details of the algorithm may refer to [17], for instance.

Let us consider the following metric associated with the mechanism effectiveness:

$$\mathcal{E} = -\frac{\displaystyle\int_{\Gamma_{out}} q_{out} \cdot u}{\displaystyle\int_{\Gamma_{in}} q_{in} \cdot u} \times 100\% \,. \tag{4.7}$$

In addition, we set $\mathcal{D} = \Omega$. The domains $\Omega^\star$ and ω are represented by dark and light grays, respectively. The domain ω remains unchanged throughout the optimization process. The thick lines represents Dirichlet boundary condition, while dashed lines means symmetry conditions. If nothing is specified, there is homogeneous Neumann boundary condition.

The contrast on the material property is given by $\rho_0 = 3 \times 10^{-3}$. The mechanisms are manufactured using Nylon. Then, the Young's modulus is $E = 3 \times 10^3$ MPa, the Poisson ratio is $\nu = 0.4$ and the threshold stress is $\overline{\sigma} = 40$ MPa. In addition, the mechanical problem is discretized into linear triangular finite elements and three steps of uniform mesh refinement were performed during the iterative process in order to fulfill the optimality condition (4.6).

The numerical realizations are driven as follows. We start by setting the stress constraints penalty parameter $\alpha = 0$. Then, for a given volume penalty $\beta^\star$, we set the in-out weight parameter κ as large as possible in order to get a functional mechanism. This procedure leads to very flexible configurations endowed with hinges where the stresses in general blow-up. Finally, the process is restarted with the same $\beta^\star$ and κ parameters as before, while the parameter α is turn-on and chosen so that the stress constraints are satisfied.

4.1. **Example 1.** Let us consider a moonie mechanism design, which transforms an horizontal input force into a vertical output displacement. The hold-all domain, representing the initial guess, is a square of dimensions 50×50 mm^2. It is modeled using double symmetry conditions and an initial mesh with 1568 elements and 837 nodes. The moonie is submitted to two uniformly distributed loading q_{in} and q_{out}, as shown in Fig. 3. The input load is given by $q_{in} = -20$ N/mm^2. The stiffness of the exterior medium is represented by $K = 100$ N/mm and the desired output displacement is $u_{out} = 1$ mm, so that the output load is $q_{out} = -10$ N/mm^2. Finally, we chose $\beta^\star = 50$ and $\kappa = 2.0$.

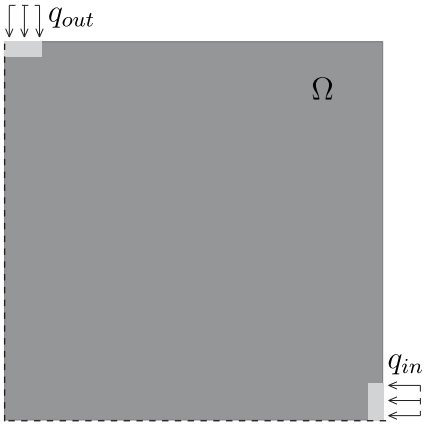

FIGURE 3. Example 1: Initial guess and boundary conditions.

In Fig. 4 the stress distributions obtained at the end of the optimization process are presented. The unconstrained case ($\alpha = 0$) has been obtained after 28 iterations. We note that the maximum stress is more than twice the admissible threshold due to the presence of hinges, as can be seen in Fig. 4(a). On the other hand, for the constrained case ($\alpha = 2$) the stress is under control and the final topology is free of hinges, as shown in Fig. 4(b). This result has been obtained after 24 iterations. The maximal stress for both cases obtained at the end of the iterative process are presented in Table 1. The amplified deformed configurations are presented in Figs. 5(a) and 5(b)

for the unconstrained and constrained cases, respectively. Finally, the graphic in Fig. 6 shows the effectiveness $\mathcal{E}$ during the iterative process for both cases.

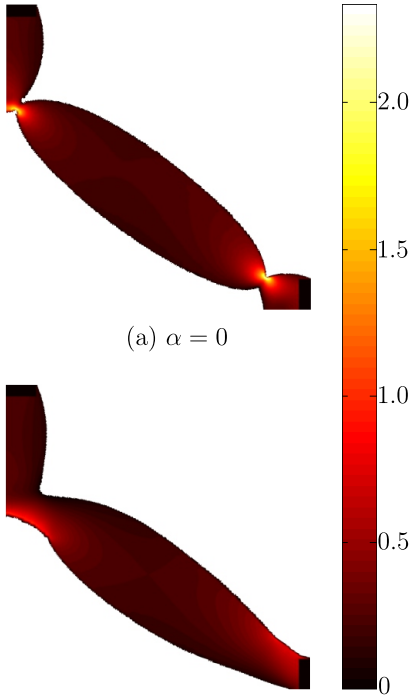

(a) $\alpha = 0$

(b) $\alpha = 2$

FIGURE 4. Example 1: Stress distributions for the unconstrained (a) and constrained (b) cases.

TABLE 1. Example 1: Maximal normalized stress obtained at the end of the iterative process.

	$\alpha = 0$	$\alpha = 2$
$\max_{\Omega}(S_M)$	2.3334	1.0211

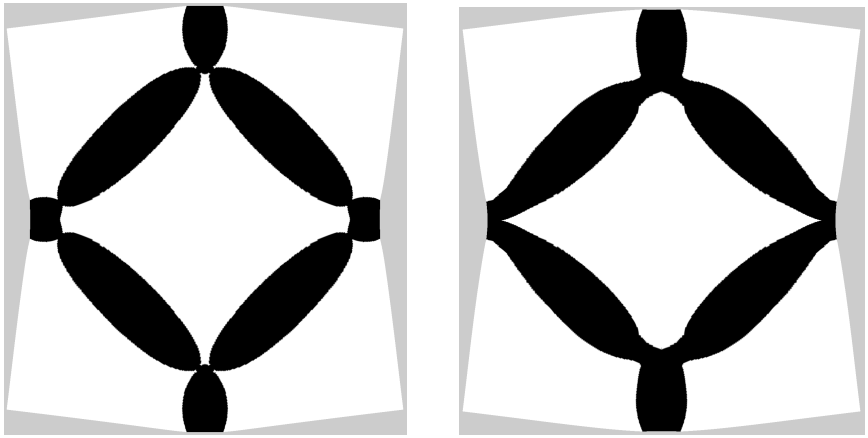

(a) $\alpha = 0$ (b) $\alpha = 2$

FIGURE 5. Example 1: Amplified deformed configurations for the unconstrained (a) and constrained (b) cases.

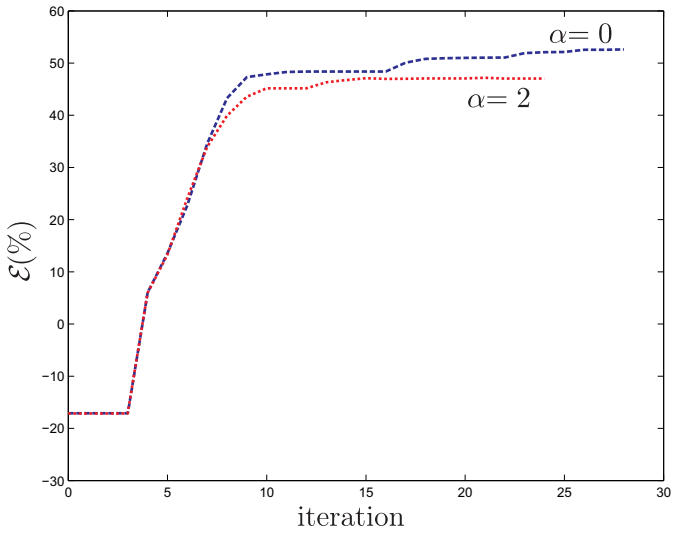

FIGURE 6. Example 1: Effectiveness $\mathcal{E}$ during the iterative process.

4.2. **Example 2.** This example consists in an inverter mechanism design. In this case, the hold-all domain representing the initial guess is a rectangle of dimensions 100×50 mm^2 clamped on the left corner of length 5 mm. It is also modeled using horizontal symmetry conditions. The initial mesh has 3356 elements and 1764 nodes. The inverter is submitted to two uniformly distributed loading $q_{in} = 10$ N/mm^2 and $q_{out} = 5$ N/mm^2, see Fig. 7. The stiffness of the exterior medium is set as $K = 100$ N/mm. Therefore, the desired output displacement is given by $u_{out} = -0.5$ mm. Finally, we chose $\beta^\star = 100$ and $\kappa = 9.0$.

FIGURE 7. Example 2: Initial guess and boundary conditions.

The stress distributions obtained at the end of the optimization process are presented in Fig. 8. Similarly to the first example, the maximum stress associated with the unconstrained case ($\alpha = 0$) exceeds the admissible threshold due to the presence of hinges, as shown in Fig. 8(a). This result has been obtained after 48 iterations. On the other hand, in the constrained case ($\alpha = 10$) the stress is under control and the final topology is free of hinges, as can be seen in Fig. 8(b). In this case, the optimal design has been obtained after 37 iterations. Furthermore, the maximal stress for both considered cases obtained at the end of the iterative process are presented in Table 2. The amplified deformed configurations are presented in Figs. 9(a) and 9(b) for the unconstrained and constrained cases, respectively. We observe that the obtained mechanisms perform the desired movements. Finally, the effectiveness $\mathcal{E}$ during the iterative process for both cases are presented in Fig. 10.

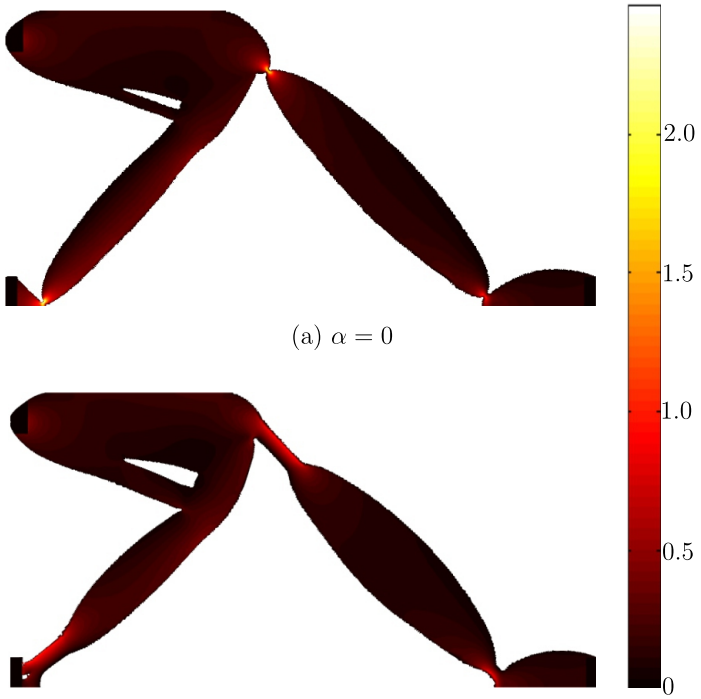

(a) $\alpha = 0$

(b) $\alpha = 10$

FIGURE 8. Example 2: Stress distributions for the unconstrained (a) and constrained (b) cases.

TABLE 2. Example 2: Maximal normalized stress obtained at the end of the iterative process.

	$\alpha = 0$	$\alpha = 10$
$\max_{\Omega}(S_M)$	2.46	1.0178

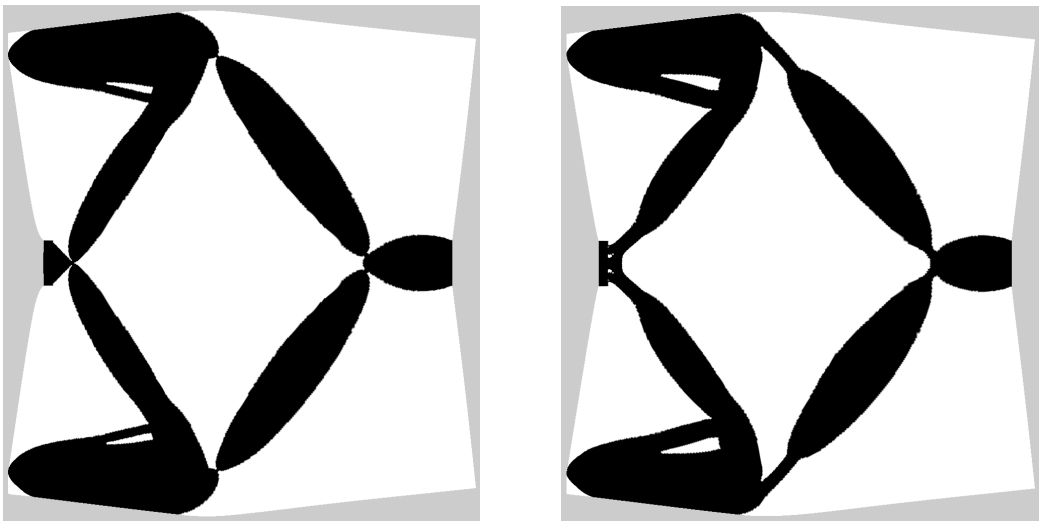

(a) $\alpha = 0$ (b) $\alpha = 10$

FIGURE 9. Example 2: Amplified deformed configurations for the unconstrained (a) and constrained (b) cases.

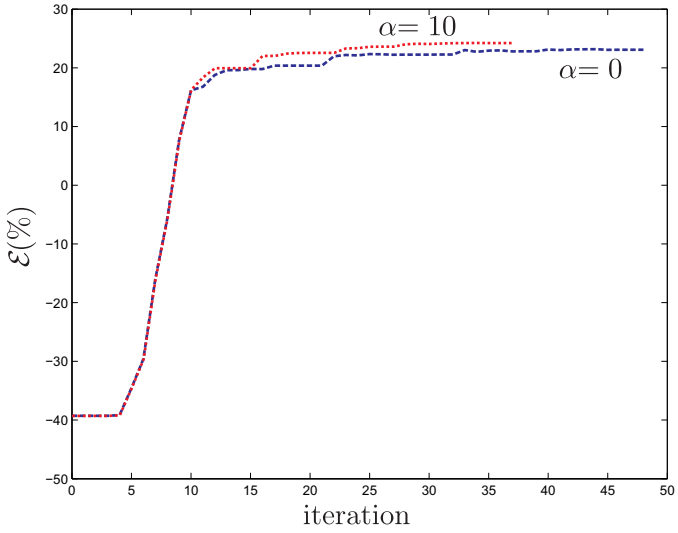

FIGURE 10. Example 2: Effectiveness $\mathcal{E}$ during the iterative process.

4.3. **Example 3.** In this last example the design of a pliers mechanism is considered. The hold-all domain, representing the initial guess is given by a rectangle of dimensions 100×50 mm^2 with a jaw, as shown in Fig. 11. It is modeled using horizontal symmetry conditions and an initial mesh with 2832 elements and 1489 nodes. The stiffness of the exterior medium is given by $K = 100$ N/mm and the desired output displacement is set as $u_{out} = -0.2$ mm. Therefore, the pliers is submitted to two uniformly distributed loading $q_{in} = -20$ N/mm^2 and $q_{out} = 4$ N/mm^2. Finally, we chose $\beta^\star = 35$ and $\kappa = 9.0$.

FIGURE 11. Example 3: Initial guess and boundary conditions.

The Fig. 12 shows the obtained stress distributions for both considered cases at the end of the optimization process. The result for unconstrained case ($\alpha = 0$) has been obtained after 57 iterations. The maximum stress is almost three times the admissible threshold due to the presence of hinges, as can be seen in Fig. 12(a). On the other hand, in the constrained case ($\alpha = 4$) the stress remains under control, as shown in Fig. 12(b). In this case, the result has been obtained after 43 iterations. It is interesting to note that the hinge where the stress blows-up in Fig. 12(a) becomes an arc-shaped spring in Fig. 12(b), allowing to keep the maximal stress close to the threshold. The maximal stress for both cases obtained at the end of the iterative process are presented in Table 3. The amplified deformed configurations are presented in Figs. 13(a) and 13(b) for the unconstrained and constrained cases, respectively. Finally, the graphic in Fig. 14 shows the effectiveness $\mathcal{E}$ during the iterative process for both cases. Since the hinge is replaced by an arc-shaped spring, the

effectiveness for $\alpha \neq 0$ becomes slice less than for $\alpha = 0$, but the functionality of both mechanisms is attended.

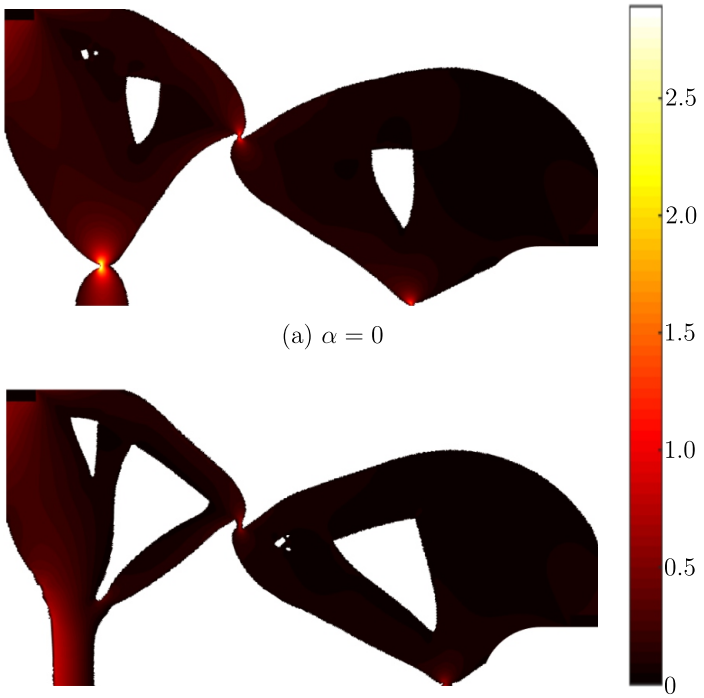

(a) $\alpha = 0$

(b) $\alpha = 4$

FIGURE 12. Example 3: Stress distributions for the unconstrained (a) and constrained (b) cases.

TABLE 3. Example 3: Maximal normalized stress obtained at the end of the iterative process.

	$\alpha = 0$	$\alpha = 4$
$\max_{\Omega}(S_M)$	2.8922	0.8767

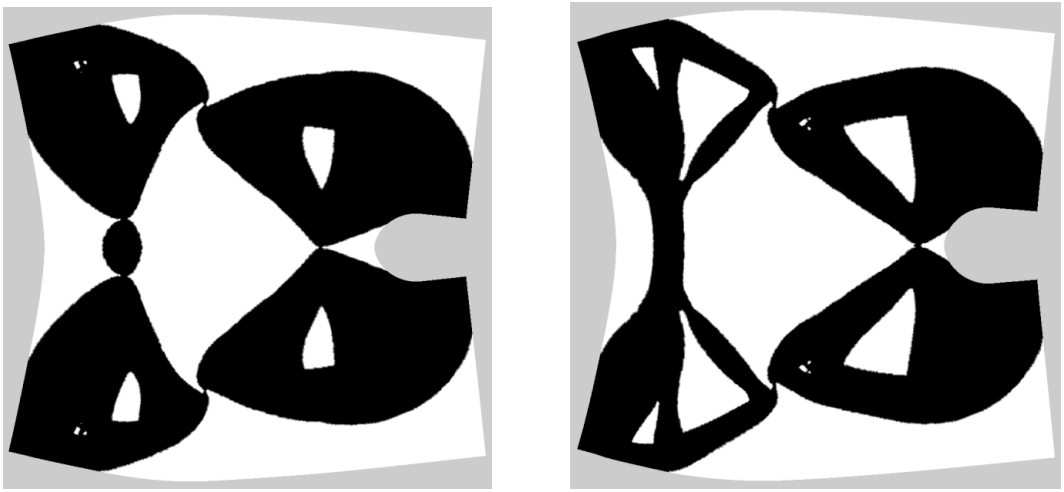

(a) $\alpha = 0$ (b) $\alpha = 4$

FIGURE 13. Example 3: Amplified deformed configurations for the unconstrained (a) and constrained (b) cases.

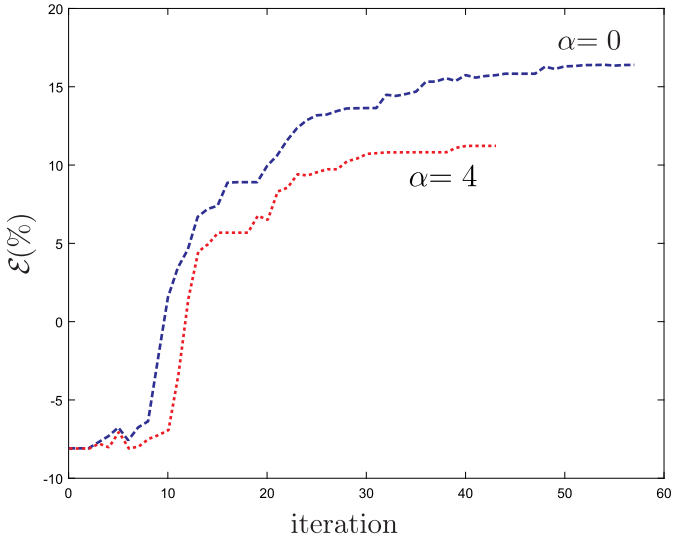

FIGURE 14. Example 3: Effectiveness $\mathcal{E}$ during the iterative process.

5. Conclusion

In this paper a novel approach to topology design of compliant mechanisms under von Mises stress constraints has been presented. It relies on an efficient and simple computational procedure based on the topological derivative concept and a level-set domain representation method. In order to deal with the local constraints, a class of von Mises stress penalty functions has been used. Finally, some numerical examples have been presented, showing that the proposed approach naturally keeps the stress under control by avoiding the undesirable flexible joints (hinges). In particular, the numerical examples agree well with the results that should be expected by other methods. Therefore, our approach can be seen as an alternative method for optimum design of compliant mechanisms under stress constraints.

Acknowledgements

This research was partly supported by CNPq (Brazilian Research Council), CAPES (Brazilian Higher Education Staff Training Agency) and FAPERJ (Research Foundation of the State of Rio de Janeiro). These supports are gratefully acknowledged.

References

[1] G. Allaire, F. Jouve, and H. Maillot. Minimum stress optimal design with the level-set method. *Engineering Analysis with Boundary Element*, 32(11):909–918, 2008.

[2] H. Ammari and H. Kang. *Polarization and moment tensors with applications to inverse problems and effective medium theory*. Applied Mathematical Sciences vol. 162. Springer-Verlag, New York, 2007.

[3] S. Amstutz. Sensitivity analysis with respect to a local perturbation of the material property. *Asymptotic Analysis*, 49(1-2):87–108, 2006.

[4] S. Amstutz. A penalty method for topology optimization subject to a pointwise state constraint. *ESAIM: Control, Optimisation and Calculus of Variations*, 16(3):523–544, 2010.

[5] S. Amstutz. Analysis of a level set method for topology optimization. *Optimization Methods and Software*, 26(4-5):555–573, 2011.

[6] S. Amstutz and H. Andrä. A new algorithm for topology optimization using a level-set method. *Journal of Computational Physics*, 216(2):573–588, 2006.

[7] S. Amstutz and A. A. Novotny. Topological optimization of structures subject to von Mises stress constraints. *Structural and Multidisciplinary Optimization*, 41(3):407–420, 2010.

[8] S. Amstutz, A. A. Novotny, and E. A. de Souza Neto. Topological derivative-based topology optimization of structures subject to Drucker-Prager stress constraints. *Computer Methods in Applied Mechanics and Engineering*, 233–236:123–136, 2012.

[9] S. Amstutz, A. A. Novotny, and N. Van Goethem. Topological sensitivity analysis for elliptic differential operators of order $2m$. *Journal of Differential Equations*, 256:1735–1770, 2014.

[10] R. Ansola, E. Veguería, J. Canales, and J. A. Tárrago. A simple evolutionary topology optimization procedure for compliant mechanism design. *Finite Elements in Analysis and Design*, 44:53–62, 2007.
[11] R. H. Burns and F. R. E. Crossley. Kinetostatic synthesis of flexible link mechanisms. *ASME-Paper*, 68(36), 1964.
[12] E. L. Cardoso and J. S. O. Fonseca. Strain energy maximization approach to the design of fully compliant mechanisms using topology optimization. *Latin American Journal of Solids and Structures*, (1):263–275, 2004.
[13] D. M. De Leon, J. Alexandersen, J. S. O. Fonseca, and O. Sigmund. Stress-constrained topology optimization for compliant mechanism design. *Structure Multidisciplinary Optimization*, 2015.
[14] H. A. Eschenauer and N. Olhoff. Topology optmization of continuum structures: a review. *Applied Mechanics Reviews*, 54(4):331–390, 2001.
[15] C. Le, J. Norato, and T. Bruns. Stress-based topology optimization for continua. *Structural Multidisciplinary Optimization*, 41:605–620, 2010.
[16] E. Lee and H. C. Gea. A strain based topology optimization method for compliant mechanism design. *Structure and Multidisciplinary Optmization*, 49:199–207, 2014.
[17] C. G. Lopes, R. B. dos Santos, and A. A. Novotny. Topological derivative-based topology optimization of structures subject to multiple load-cases. *Latin American Journal of Solids and Structures*, 12:834–860, 2015.
[18] J. Luo, Z. Luo, S. Chen, L. Tong, and M. Yu Wang. A new level set method for systematic design of hinge-free compliant mechanisms. *Computer Methods in Applied Mechanics and Engineering*, (198):318–331, 2008.
[19] L. R. Meneghelli and E. L. Cardoso. Design of compliant mechanisms with stress constraints using topology optimization. *Optimization of Structures and Components, Advanced Structured Materials*, 43, 2013.
[20] A. A. Novotny and J. Sokołowski. *Topological derivatives in shape optimization*. Interaction of Mechanics and Mathematics. Springer-Verlag, Berlin, Heidelberg, 2013.
[21] O. Sigmund. On the design of compliant mechanisms using topology optimization. *Mechanics of Structures and Machines: An International Journal*, 25(4):493–524, 1997.
[22] J. Sokołowski and A. Żochowski. On the topological derivative in shape optimization. *SIAM Journal on Control and Optimization*, 37(4):1251–1272, 1999.

(C.G. Lopes & A.A. Novotny) Laboratório Nacional de Computação Científica LNCC/MCT, Coordenação de Matemática Aplicada e Computacional, Av. Getúlio Vargas 333, 25651-075 Petrópolis - RJ, Brasil
Email address: novotny@lncc.br